

Sensitivities of an intense Mediterranean cyclone: Analysis and validation

By VICTOR HOMAR* and DAVID J. STENSRUD

NOAA/National Severe Storms Laboratory, Norman, Oklahoma, USA

(Received 23 May 2003; revised 18 November 2003)

SUMMARY

On 10 and 11 November 2001 a deep cyclone moved northward across the western Mediterranean. Severe floods affected Algeria on 10 November and a mesoscale-sized region of strong damaging winds occurred over the Balearics and eastern Spain during the first hours of 11 November. These large intense cyclones, originating over north Africa and moving northward, are occasionally observed in the region. Numerical simulations of these types of events are potentially hampered by the lack of observations over the Mediterranean Sea, north Africa and the Atlantic Ocean. To evaluate more accurately the regions in which the model simulations are influenced by this lack of data, the MM5 adjoint system is used to determine the most sensitive areas within the initial conditions of the simulation of this 10–11 November event. Limitations of available adjoint models, such as their linear character, suggest that a test of the applicability of MM5 to the case under analysis is needed. In this study, the evaluation is performed by means of the tangent linear model and, despite finding that the adjoint has an acceptable accuracy, important nonlinear effects are found and attributed to the moist processes. The study tracks backward in time the sensitivities shown at different simulation times using parameters chosen to characterize the cyclone's intensity at 0000 UTC 11 November. Results reveal that the areas that show the largest sensitivities are located over north Africa for the 12 h and 24 h simulations, whereas south-western and western Europe emerge as areas with important sensitivities for the longer 36 h and 48 h simulations. Subsynoptic details regarding the shape and intensity of an upper-level trough, as well as a low-level cold front, are highlighted by the adjoint runs as the structures which influence most strongly the baroclinic development of the intense Mediterranean cyclone and the damaging surface winds it produces. The usefulness of the sensitivity fields in the nonlinear simulations is confirmed by perturbing the control model's initial conditions using the adjoint results as guidance. This analysis helps to quantify the limitations of the linear estimation when applied to the full nonlinear model, focusing on the nonlinearities introduced by the moist physics parametrizations.

KEYWORDS: Adjoint model

1. INTRODUCTION

The Mediterranean region is a very active cyclogenetic area. Its orography is an important agent in favoring cyclogenesis and in modifying the location and evolution of the cyclones. Its location in the mid-latitudes exposes the region to invasions of both polar and subtropical air masses, promoting baroclinically unstable environments (Fig. 1). Although most cyclones are not significant in the sense of producing hazardous weather, Jansà *et al.* (2001) show for the western Mediterranean that in more than 94% of the heavy precipitation events, a cyclonic centre is present within 600 km. In addition, the strong winds associated with intense cyclones cause large economic losses and even casualties. A particularly damaging type of cyclone is the north African baroclinic low. A conceptual model of this type of cyclone emerges from the studies of Arreola *et al.* (2003) and Homar *et al.* (2002): they originate over north Africa when a cold Atlantic intrusion is present at low levels and a deep tropopause fold is present at high levels. The surface low then moves to the north, steered by the upper-level trough, and rapidly deepens as it reaches the Mediterranean Sea. Diabatic heating from condensation is frequently determinant in Mediterranean cyclones (Shay-El and Alpert 1991) and is also found to play a role in these events. As a result, catastrophic personal and economic damages are produced by strong winds and floods across the western Mediterranean basin.

Producing an accurate numerical forecast of these events is a challenging task, typically hampered by the lack of observations over the Atlantic Ocean, north Africa,

* Corresponding author: NOAA/National Severe Storms Laboratory, 1313 Halley Circle, Norman, OK, 73069, USA. e-mail: Victor.Homar@noaa.gov

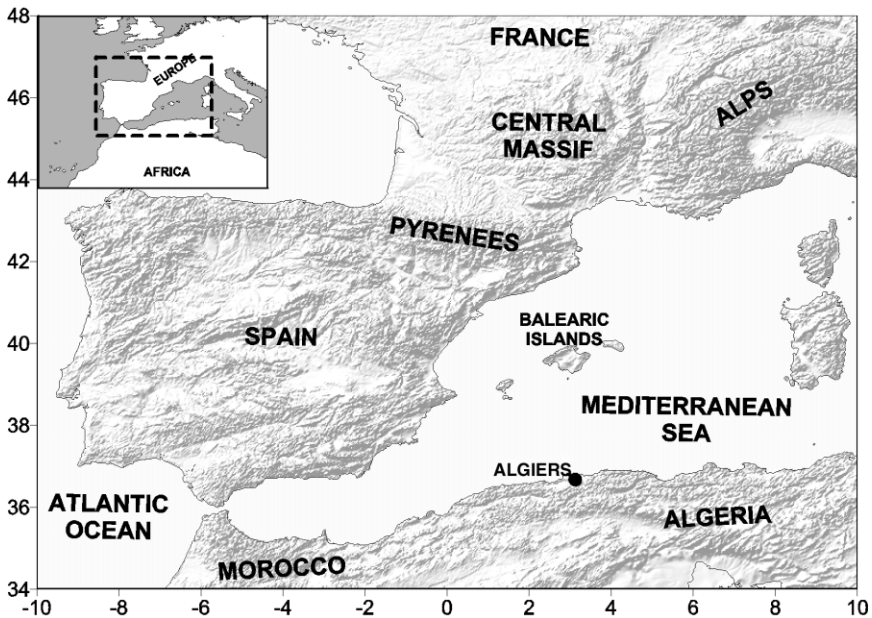


Figure 1. Topography of the western Mediterranean Sea.

and the Mediterranean Sea. Although models generally succeed in reproducing the African baroclinic zone and its northern movement, the low centre and the associated wind and rainfall bands are frequently misplaced. To assist forecasters in making warning decisions, a good numerical forecast of these aspects is especially important in the highly populated areas of the western Mediterranean basin.

Improving the accuracy of forecasts has been an everpresent challenge since the dawn of numerical prediction. Presently, many efforts are aimed at improving forecasts by incorporation of new data sources that seem likely to lead to more accurate analyses. A simple approach to improve the model input fields is a general increase of observations across the area covered by the model domain. However, sensitivity analysis offers a more efficient (and cheaper) approach to this problem. The identification of the upstream features which most affect a particular forecast aspect has great interest in numerical prediction and it could provide valuable guidance in designing an efficient observation strategy. This approach is conceptually similar to targeting observations (e.g., Snyder 1996; Langland 1999; Langland *et al.* 1999a), but differs in that the end result is not necessarily an observation strategy for a single event but the identification of a region in which an enhanced routine observing network could be deployed during the autumn, when the western Mediterranean cyclones are most destructive. Sensitivities also allow the evaluation of the potentially degrading effects in a numerical forecast of poorly analysed regions in the initial fields. In addition, the sensitivity analysis approach has been successfully used as a guide to build sets of perturbations in an ensemble numerical prediction framework (Molteni *et al.* 1996; Xu *et al.* 2001).

The traditional sensitivity analysis procedure, in which the effect of modifications in the control run are traced throughout the simulation, allows one to obtain the nonlinear sensitivities of all forecast aspects to the modifications. Theoretically, an extremely large number of experiments is required in order to find the optimal perturbation that maximizes the change in the forecast aspects using this approach. However, the adjoint

model of the tangent linearization to the full nonlinear model provides an excellent framework to determine the sensitivities of a particular forecast feature of interest, called an aspect or *response function J* (Errico 1997). Given a particular response function, the adjoint traces back its sensitivity, computing the gradients of the response function with respect to the model state (i.e., the set of forecast fields in the forward model). When the adjoint is integrated backwards to the initial time, we obtain the gradient of the response function to the initial and boundary conditions. The traditional and the adjoint methodologies are essentially inverse strategies: whereas the traditional approach allows one to evaluate the effect of *one* perturbation to *any number* of response functions, the adjoint allows one to evaluate the effect of *any* perturbation to *one particular* response function. Alpert *et al.* (1996) discussed the differences between the traditional approach, using the factor-separation technique, and the adjoint method for a Mediterranean cyclogenesis event. Besides four-dimensional variational data assimilation, the most common application of adjoint models is the analysis of forecast error sensitivities and the detection of regions in the analysis fields which show the largest sensitivity. Furthermore, the sensitivity fields provide good guidance on the size and shape of the perturbations that minimize the forecast error (Errico 1997; Langland *et al.* 2002).

However, the application of the adjoint model has limitations which must be considered carefully. Sensitivity analyses should always be accompanied by a measure of validity. Since the adjoint is the transpose operator of the tangent linear model, its results are also tangent linear and no information can be deduced about the sensitivities of the nonlinear evolution of these perturbations. Thus, it is necessary to test the accuracy of the tangent linear model for each sensitivity experiment (Errico *et al.* 1993). This is particularly important when moist physics and convection strongly influence the forecast of the response function (Errico and Raeder 1999) because the linear approximation to the full model can fail critically. For example, diabatic processes hamper the moist tangent linear model accuracy by frequent discontinuous transitions represented by on–off switches (Vukićević and Errico 1993; Park and Droegemeier 1997; Errico and Raeder 1999). Thus, when moisture is considered, the actual sensitivities can be governed by the nonlinear gradients and the significance of the adjoint results is then very limited. Despite these limitations, previous studies present notable contributions based on adjoint model results. Dry adjoints are typically preferred, though moisture and implicit convection are successfully used in some studies. Langland *et al.* (1999a,b) showed an application of adjoints to targeting adaptive observations for cyclones during the Fronts and Atlantic Storms Experiment. Some studies have used the adjoint results to analyse the cause–effect mechanisms in cyclogenesis (Errico and Vukićević 1992), mesoscale convective systems (Xu *et al.* 2001) and the return flow over the Gulf of Mexico (Lewis *et al.* 2001).

The aim of the present work is to determine the areas in which the simulation of a destructive north African western Mediterranean cyclone shows the highest sensitivities. Since diabatic heating from condensation is important in these cyclogenetic cases, and neglecting moist physics could lead to serious deficiencies in the adjoint model results (Toth and Kalnay 1993), a moist adjoint model is used and the accuracy of this model is evaluated. Numerical details of the nonlinear and adjoint experiments are described in section 2. Section 3 presents a synoptic overview of the case. An analysis of the validity of the linear adjoint results in the nonlinear model is discussed in section 4. Section 5 shows the response functions used to characterize some aspects of the cyclone and presents the sensitivity fields obtained from the adjoint, as well as the effects of its derived perturbations in the nonlinear model. Conclusions and final remarks are found in section 6.

2. NUMERICAL CONFIGURATION

(a) *Nonlinear experiments*

The Pennsylvania State University–National Center for Atmospheric Research (Penn State–NCAR) non-hydrostatic mesoscale modelling system version 5 (MM5) (Grell *et al.* 1995; Dudhia *et al.* 2002; Zou *et al.* 1997, 1998) is used to perform all the simulations presented in this study. There exist substantial differences between the standard nonlinear MM5 system and the adjoint. A limited number of physical parametrization scheme options are available in the adjoint code, and the number of available options is even less in the tangent linear model.

The domain configuration is a compromise between the resolution needed to resolve well the mesoscale-sized damaging aspects of the cyclone and the limitations imposed by the adjoint system. A single grid of 71×71 points, at 60 km resolution, which covers all the western Mediterranean, north Africa, the north-west Atlantic Ocean and Europe is used (Fig. 2). This resolution might not adequately represent some mesoscale features of the cyclone but it is intended to be useful in analysing its synoptic and large subsynoptic-scale sensitivities. In fact, the linear character of the adjoint system becomes a potential hindrance on the mesoscale, where nonlinear processes often are dominant and so high resolution runs using current adjoints are likely to be less valuable. In the vertical, 23 σ levels, with higher density at low altitudes, are used. Although a 180 s time step is used in the nonlinear MM5, the poorer diffusion scheme and physical parametrizations available in the adjoint requires the use of a shorter 120 s time step to avoid numerical instabilities. In order to analyse how the areas of sensitivity of the cyclone at a particular time change with integration duration, four time-spans are used during the study: 12, 24, 36 and 48 hours.

The standard nonlinear MM5 includes many different options for the various physical parametrization schemes. For the present study, a set of parametrizations consistent with those available in the adjoint have been chosen. The Grell *et al.* (1995) convective parametrization scheme is used. It performs well in balancing the resolved scale and the convective rainfall. The resolved-scale moist processes follow the microphysics scheme of Dudhia (1989), which includes a simple representation of cloud ice. The planetary boundary layer is parametrized using the Blackadar scheme (Zhang and Anthes 1982). This scheme distinguishes between the so-called nocturnal (stable, mechanically driven turbulence and forced convection) and the day-time free-convection boundary-layer regimes. Sea surface temperatures remain constant during the simulation and are taken from the National Centers for Environmental Prediction (NCEP) weekly analysis. A simple radiative-cooling scheme is selected, which accounts for long-wave and short-wave interactions with clouds and clear air (Benjamin 1983). Initial and boundary conditions are built from the NCEP global $2.5^\circ \times 2.5^\circ$ fields, reanalysed to the model domain grid by means of a Cressman-type objective analysis ingesting standard surface and upper-air observations. Time-dependent boundary conditions are supplied to the simulation by means of a relaxation inflow/outflow five-point sponge frame. An upper radiative condition is used to minimize spurious noise reflection at the model top.

(b) *Tangent and adjoint experiments*

Tangent (TGL) and adjoint (ADJ) linear models are linear operators which are applied to perturbations of the basic nonlinear state. It is important to recognize that these models are not linearizations of the full nonlinear model, but are instead linear approximations to the nonlinear equations of the evolution of perturbations (i.e., tangent linear). In fact, these linear models are integrated (forwards or backwards) along the

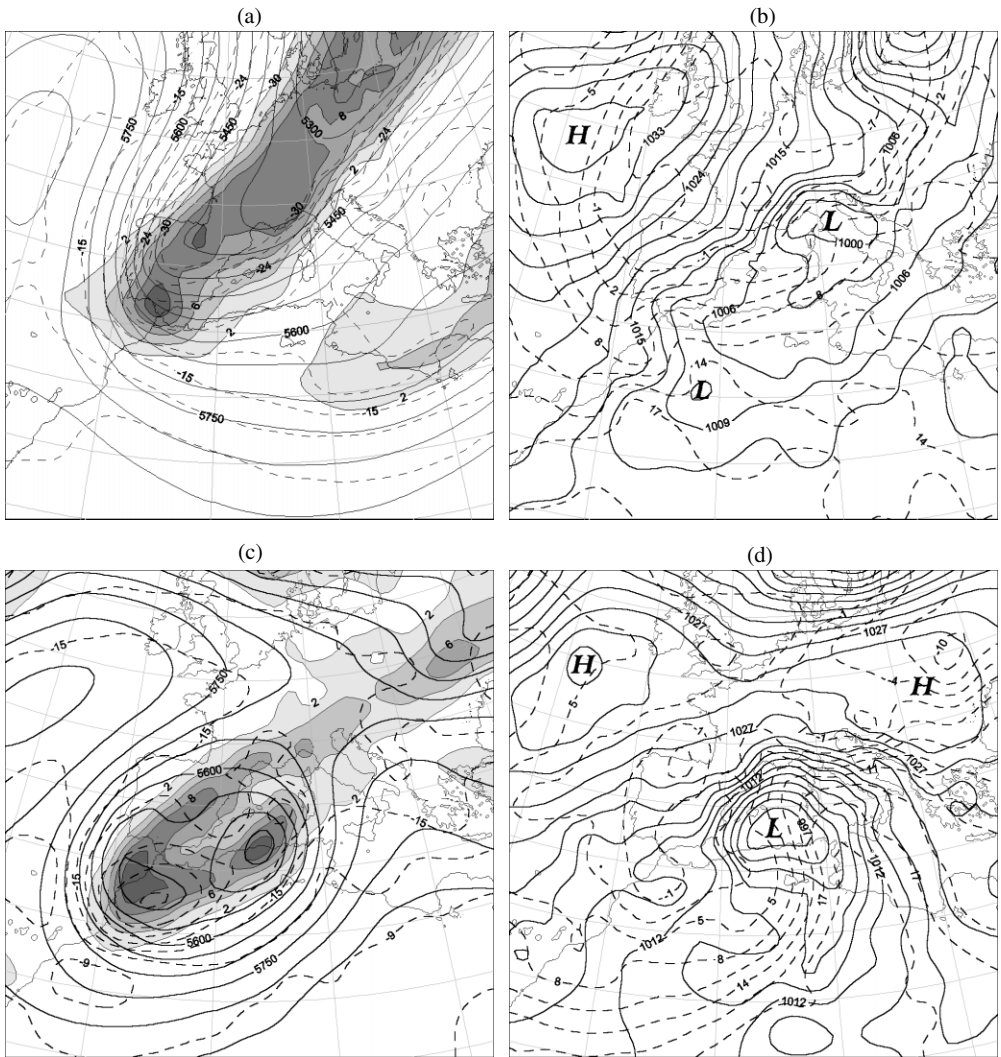


Figure 2. US National Centers for Environmental Prediction initial fields re-analysed to a 60 km grid: (a) 1200 UTC 9 November 2001, 500 hPa geopotential height (m) (solid lines), 500 hPa temperature ($^{\circ}\text{C}$) (dashed lines) and 250 hPa potential vorticity ($\text{PVU} = 10^{-6} \text{ K m}^2 \text{ s}^{-1} \text{ kg}^{-1}$) (stippled); (b) 1200 UTC 9 November 2001, sea-level pressure (hPa) (solid lines) and 850 hPa temperature ($^{\circ}\text{C}$) (dashed lines); (c) 0000 UTC 11 November 2001, 500 hPa geopotential height (m) (solid lines), 500 hPa temperature ($^{\circ}\text{C}$) (dashed lines) and 250 hPa potential vorticity ($\text{PVU} = 10^{-6} \text{ K m}^2 \text{ s}^{-1} \text{ kg}^{-1}$) (stippled), and (d) 0000 UTC 11 November 2001, sea-level pressure (hPa) (solid lines) and 850 hPa temperature ($^{\circ}\text{C}$) (dashed lines).

nonlinear trajectory followed by the basic state. Although the TGL and ADJ are linear operators, their coefficients depend on the (nonlinear) basic-state trajectory and change every time step. Thus, the computation and storage of the full basic-state trajectory is needed before running the TGL or ADJ models. Although the accuracy of the TGL was affected little by the frequency of update of the basic state for long (24 h or longer) simulations in the case of dry runs (Errico *et al.* 1993), we use an every-time-step update to avoid any degradation from this source for a situation in which moisture and convection play a large role. Thus, rapid changes in the basic state are properly accounted for in the evolution of perturbations in the linear runs.

Since the ADJ is an exact adjoint operator of the TGL operator (Zou *et al.* 1998), the validation can be processed by checking the accuracy of the TGL against the forward model run using the same settings. The TGL code currently available includes a more limited set of physics options than the ADJ. Thus, a Kuo (1974) type convective parametrization must be used instead of the Grell scheme. Furthermore, the explicit moisture scheme of Dudhia is not available; the large-scale saturation is simply removed instead. These limitations to the TGL are important for the later validation of the adjoint system.

Therefore, two different sets of model configuration are used: one with the Grell scheme and the explicit Dudhia microphysics, only available for the ADJ and nonlinear models to study the cyclone sensitivities; and a second using the Kuo scheme and simple stable precipitation, to evaluate the ADJ performance. Section 4 shows further details on the testing and validation procedures used in the present study.

3. SYNOPTIC OVERVIEW

The case of 9–11 November 2001 has been selected as a recent example of an intense Mediterranean cyclone of African origin. Arreola *et al.* (2003) presented a detailed analysis of the mechanisms involved in the event. During 9 and 10 November more than 900 people were killed*, thousands injured and about 23 000 homes destroyed from damaging winds and severe flash floods in Algeria. Strong winds and persistent rainfall also affected the Balearic Islands on 11 November, producing 4 casualties, the uprooting of about 220 000 pines and the removal of 60% of beach sand. A total of more than €100 million in private property damage was estimated by insurance companies.

The synoptic situation on 1200 UTC 9 November 2001 shows a large positively tilted upper-level cold trough covering Europe and extending south toward north Africa (Fig. 2(a)). A tropopause fold linked to the trough is identifiable on the potential vorticity (PV) field at 250 hPa. Weak sea level pressure values over the western Mediterranean are associated with a secondary upper-level wave extending from south-eastern France to Libya (Fig. 2(b)). An incipient low-pressure centre is already identifiable at this time over north Africa. The temperature field at low levels shows a cold front associated with the low, producing cold advection throughout Spain, Morocco and north Algeria. Over the next day, this cold advection persistently transports cold air southward and tightens the temperature gradient over north Africa. During this time, the upper-level trough develops a closed circulation with two embedded rotating centres (Fig. 2(c)). Under the dynamic forcing of the eastern upper-level PV centre, within a baroclinically unstable environment, an intense low-level cyclogenesis occurs over Algeria on 10 November. Then steered by the upper-level flow, the cyclone follows a northern trajectory, producing strong winds throughout the western Mediterranean basin (Fig. 2(d)). Latent heat from condensation plays an important role in sustaining the cyclone intensity during the last stages of its evolution (for details, see Arreola *et al.* (2003)). In fact, 262 mm of rainfall in 24h were reported at Algiers on 10 November and more than 400 mm were reported during the whole event at some stations on the Balearic Islands.

This analysis suggests where an accurate representation of the atmospheric state seems especially important, and even necessary, for a successful numerical prediction of the event. The upper-level trough over Europe and the low-level cold invasion over north Africa emerge as key features, and so a high sensitivity of the later Mediterranean cyclone to these areas is inferred. The adjoint model provides a way to evaluate these

* See <http://www.em-dat.net/>

hypotheses and to quantify the sensitivity fields, giving the opportunity to assess the relative roles of different fields and vertical levels for different simulation times.

4. VALIDATION

Before performing a sensitivity analysis on any particular simulation, an evaluation of the adjoint model accuracy must be made and the validity of the sensitivity fields in the full nonlinear forward model (FWD) must be tested. Since the ADJ is derived from the TGL, the greatest limitation in the application of its results is their linear character. When the tangent linear model is able to reproduce the dominant modes of the nonlinear simulation, the adjoint results will successfully describe the sensitivities of the nonlinear model. However, if nonlinear processes govern the evolution of the perturbations, the linear models will not describe the sensitivities adequately. In this case, the nonlinear sensitivities are more likely to be larger than the linear ones and the usefulness of the adjoint results is limited. The ability of the TGL to describe the nonlinear evolution of perturbations depends on the magnitude of the perturbations, which varies with integration time and physical processes involved in each case. Several approaches have been used in other studies to address this issue (Park and Drogemeier 1997). A common validation method consists of testing the accuracy of the TGL by comparing it with the FWD results. Since the adjoint operator is an exact transpose of the TGL operator, its applicable range will be that of the TGL. Errico *et al.* (1993) used the correlation as a measure of similarity between forecast perturbations determined from TGL and nonlinear runs to show the high accuracy of a dry TGL.

Since the tangent linear code for the Grell convective scheme and Dudhia microphysical parametrization scheme are currently not available*, the results obtained using this model configuration cannot be tested using the TGL–FWD correlation method. Instead, we infer the accuracy of the ADJ results from tests performed using the TGL with the Kuo convective scheme and a simple stratiform condensation parametrization. We assume that the Grell–Dudhia schemes behave better than the Kuo simple condensation schemes. Therefore, the validity range of the latter configuration (used for the tests) is meant as a reasonable estimate of the validity range of the former (used for sensitivity calculations with the adjoint in the next section).

In principle, any kind of perturbation can be used to perform the comparison. However, in order to focus the test upon the forecast of features of the cyclone under study, we make use of a set of perturbations built from adjoint sensitivity fields. For this test, all ADJ variables are initialized to a value of one over the western Mediterranean basin in the lower half of the domain on 0000 UTC 11 November, the sensitivity time. Consequently, instead of using initial random perturbations across the domain, the test will evaluate the accuracy of the TGL when forecasting aspects of interest over the basin at this time.

Although no theoretical restrictions exist on the precise shape or location of the perturbations, we build them by using the shape and sign of the sensitivity fields $\nabla_i \mathbf{J}$ at the initial time (t_0) of the forward simulations, rescaled by the coefficients α and s_i :

$$\delta \chi_i = \alpha s_i \frac{\nabla_i \mathbf{J}(t_0)}{|\nabla_i \mathbf{J}(t_0)|_{\max}}, \quad (1)$$

* Linear subroutines for the Grell convective and Dudhia microphysical schemes are available under specific request from NCAR but these are currently not debugged and tested for public use (NCAR, personal communication).

where i refers to each model variable, s_i is the variable-dependent reference scale (i.e. 1 m s^{-1} , 1 K , 1 hPa and 1 g kg^{-1}) and α is an amplification parameter which controls the perturbation size. The parameter α is varied from -4 to $+4$ to perform the analysis over a wide spectrum of perturbation sizes. For each of the perturbations, a FWD simulation is performed and the differences with respect to the FWD control run define the nonlinear perturbation evolution. Since TGL is a linear operator, the TGL forecast perturbation for each perturbation size is α times the TGL forecast of the unitary ($\alpha = 1$) perturbation, hence only one single TGL run for each simulation time is made. Then, each nonlinear perturbation is compared to the linear estimation by computing the correlation between them. The general tendency shows that as $\|\alpha\|$ decreases, the correlations increase (Fig. 3(a)), achieving values larger than 0.93 for all time spans. However a consistent degradation of the TGL skill is obtained for very small perturbations ($\alpha < 10^{-2}$), breaking the original hypothesis regarding the validity of the linear approximation as the perturbation size decreases. This behaviour, where the linear solution does not converge uniformly to the nonlinear solution may be a symptom of a sensitivity to the model representation that reveals a structural instability in the linear operator (Kato 1980). Errico and Vukićević (1992) indicated that this occurs through excitation of highly nonlinear or discontinuous processes in the convective parametrization, such as those that depend on moist convective stability. In addition to this lack of robustness observed for small perturbations, no consistent trend in the TGL skill with simulation duration is deduced from these results. Indeed, the shortest 12 h-simulation shows the lowest correlations whereas the longest run achieves the largest correlations for small perturbations. Although nonlinear processes have more chance to occur in longer runs, the intensity of the individual nonlinear processes appears to be more influential than the number of occurrences. In particular, the cyclone deepening during the hours corresponding to the 12 h run is highly influenced by diabatic heating, such that the linearization during this period is relatively less accurate than in the longer runs, where baroclinic processes occur during most of the simulation. In addition, balancing processes occur during the first 18 h of integration, and are considered to affect the TGL and ADJ runs critically (Errico *et al.* 1993).

A second set of simulations, without the convective scheme, was performed in order to test the influence of the convective scheme on the TGL accuracy (Fig. 3(b)). In this configuration, lower correlations were obtained, though no singular behaviour was observed for the smallest α , indicating that the TGL–FWD results converge as the perturbation size decreases. This result suggests that the structural instability of the TGL observed in Fig. 3(a) at the smallest α is due to the Kuo-type convective scheme, which can produce relatively large differences in the forecast in response to small perturbations. Besides, when α is small the effect is amplified by the correlation measure because small differences between the TGL and FWD results are more important. Although the 36 h, 24 h and 12 h runs show increasing correlations as integration time decreases, the 48 h simulation still shows the largest correlation for this moist non-convective configuration.

Finally, a set of dry experiments was run in order to analyse the effect of moisture on the TGL–ADJ accuracy (Fig. 3(c)). A general increase in the correlations was found for all perturbation sizes and time spans with respect to the moist configurations, except for the 48 h run. The dry experiments present a smooth reduction in the correlations as the perturbation size and integration time increase. This indicates that a high number of nonlinear modes, related to the moist physics, are excited in the moist simulations of the Mediterranean cyclone, producing the unanticipated effects described in Fig. 3(a) and (b). In addition, these ‘moist nonlinearities’ introduce decision points (Park and

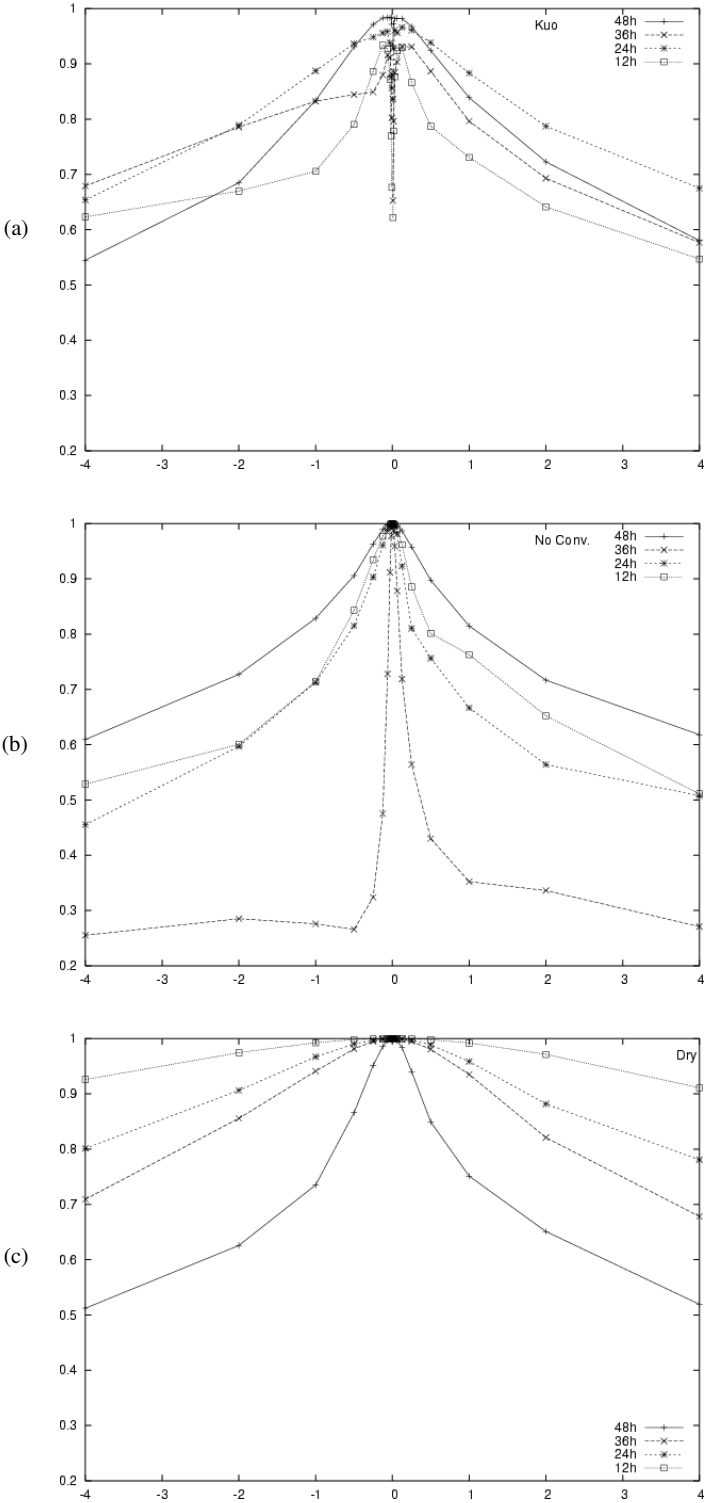


Figure 3. Correlation (vertical axis) between tangent (TGL) and forward (FWD) forecast perturbations for $-4 \leq \alpha \leq +4$ (horizontal axis) (see Eq. (1) for definition of α): (a) using simple microphysics and Kuo convective parametrization; (b) using simple microphysics but no convection scheme, and (c) dry runs.

Droegemeier 1997) in the shorter simulations, which are not crossed by the 48 h run, resulting in a failure to correctly simulate the cyclone deepening (Fig. 4). Thus, the probable reason for the higher correlations of the 48 h runs (see Fig. 3(a) and, especially, Fig. 3(b)) is the reduced complexity of the physical processes in the simulations.

Therefore, besides the singular behaviour detected for the moist processes and the convective scheme, Fig. 3(a) reveals that for this African cyclone simulation, the linear models reproduce the evolution of perturbations in the nonlinear model with acceptable accuracy (TGL–FWD correlations larger than 0.7) for perturbation sizes up to $\alpha = 1$. Thus, the fields derived from the adjoint model provide a good indication of the actual sensitivities of the forecast to perturbations to the initial conditions fields.

5. SENSITIVITY EXPERIMENTS

As previously mentioned, the response function (\mathbf{J}) is defined as an aspect of the forecast field in which we are interested, typically at a particular time (the sensitivity time, t_f). This function must be differentiable with respect to the model state components ($\boldsymbol{\chi}$), and its derivatives ($\nabla\mathbf{J}$) are indeed the variables of the adjoint model ($\hat{\boldsymbol{\chi}}$). The units of $\nabla\mathbf{J}$ are those of the particular response function we define, divided by the units of the corresponding component of the model state (i.e., m s^{-1} , $^{\circ}\text{C}$, hPa or g kg^{-1}). The integration of $\hat{\boldsymbol{\chi}}_0 = \nabla\mathbf{J}|_{t_f}$ backward provides the sensitivity of the response function with respect to the model state trajectory. In particular, when integrated until the initial time (t_0), the adjoint model indicates the change in the response function produced by any perturbation introduced to the initial conditions, i.e. the derivative of the response function at t_f with respect to the initial conditions ($\nabla\mathbf{J}|_{t_0}$). The regions of the domain with largest $\nabla\mathbf{J}|_{t_0}$ are those to which the response function is most sensitive.

The definition of the response function is an important part in any sensitivity study, but it becomes crucial when using adjoint models. A differentiable function of the model state which conveniently characterizes the forecast aspect under study is not always obvious. As discussed by Lewis *et al.* (2001), the central pressure of a cyclone or the maximum wind speed close to the cyclone are non-differentiable functions of the model state so they are not valid in the adjoint framework. Instead, the location of the feature of interest in the control run is typically used. We have defined two response functions which characterize the intensity of the cyclone: the vertical component of the relative vorticity near the surface (\mathbf{J}_1) and the surface wind speed (\mathbf{J}_2). The differentiability of the wind speed function is clear, but for the vorticity we need to express it in terms of the circulation (using Stokes's theorem) to facilitate the construction of the adjoint initial conditions in terms of u and v (Errico 1997). The response functions are

$$\mathbf{J}_1 = \iint \nabla \times \mathbf{V} \cdot \mathbf{k} \, ds \, d\sigma = \int \oint \mathbf{V} \cdot d\mathbf{l} \, d\sigma \Rightarrow \sum_{k=1,5} \sum_{A \text{ bound.}} \mathbf{V}_{i,j,k} \cdot d\mathbf{l}_{i,j,k} \quad (2)$$

and

$$\mathbf{J}_2 = \sum_B \sqrt{u_{i,j,1}^2 + v_{i,j,1}^2}. \quad (3)$$

The area A is a $600 \times 600 \text{ km}^2$ square centred at the control simulation's cyclone centre (see Fig. 5(d)) and the vertical sum extends up to $\sigma = 0.93$ ($P \simeq 900 \text{ hPa}$). The circulation term $\mathbf{V}_{i,j,k} \cdot d\mathbf{l}_{i,j,k}$ can now be easily used to initialize the adjoint model by setting to 1 (–1) the \hat{u} and \hat{v} fields at the southern (northern) and eastern (western) boundaries of area A and zero elsewhere. The subscript in the summation $\sum_{A \text{ bound.}}$ denotes summation around the whole boundary of area A . Response function \mathbf{J}_2 is only

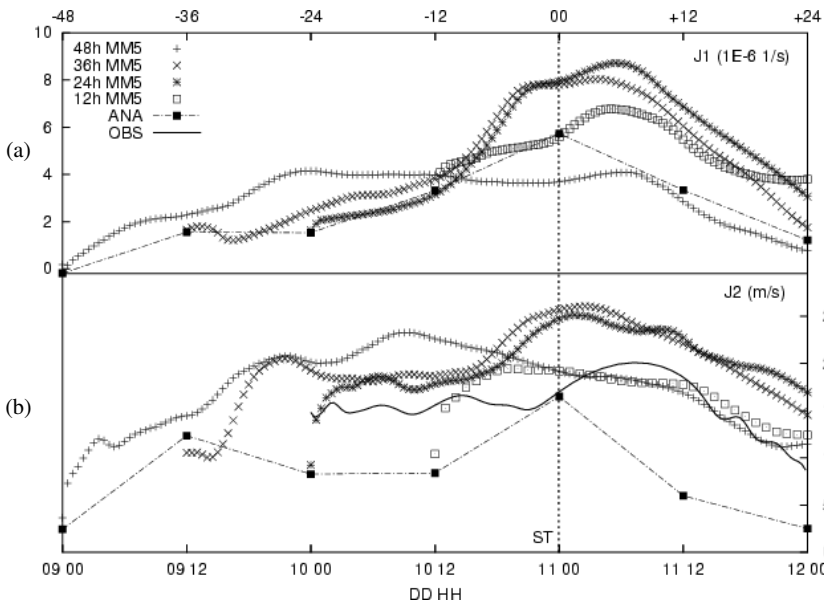


Figure 4. Response functions for the Pennsylvania State University–US National Centre for Atmospheric Research non-hydrostatic mesoscale modelling system, version 5 (MM5) control runs, and for reanalysed initial fields from the US National Centers for Environmental Prediction: (a) \mathbf{J}_1 (10^{-6} s^{-1}) and (b) \mathbf{J}_2 (m s^{-1}). See text and Eqs. (1) and (2) for definitions of \mathbf{J}_1 and \mathbf{J}_2 . Observed winds (OBS) (m s^{-1}), to permit comparison with \mathbf{J}_2 , are average values over the Balearic Islands for the times shown; times are calendar days and hours along the bottom axis and, along the top axis, are hours in relation to the sensitivity time (ST, 0000 UTC 11 November).

defined at the lowest model level, just above the surface, but the summation is over the whole of the $180 \times 120 \text{ km}^2$ area covering the Balearics (labelled B, see Fig. 8(a)).

Evaluations of \mathbf{J}_1 and \mathbf{J}_2 during the four control simulations and the reanalysed NCEP fields are shown in Fig. 4. Figure 4(a) shows an increase of \mathbf{J}_1 during days 9 and 10 for the 12 h, 24 h and 36 h runs, reaching its maximum value of over $8 \times 10^{-6} \text{ s}^{-1}$ during the first hours of 11 November. Note the differences shown by the 48 h simulation, which does not reproduce the rapid increase in circulation during 10 November. In fact, the 48 h run simulates a cyclone up to 14 hPa shallower than that in the NCEP analysis. This suggests that the 48 h simulation is following a different solution trajectory from the shorter runs. Analysis of the sensitivity for this run is especially interesting because it indicates the regions where a modification of the initial conditions can improve the forecast by shifting the solution trajectory towards the observed one. Looking at the wind speed over the Balearic Islands (\mathbf{J}_2), values reaching 23 m s^{-1} are predicted during the early hours of 10 November in the 24 h and 36 h runs. Observations averaged over the Balearic stations show that maximum wind speeds occurred during the first hours of 11 November, as is captured better by the 24 h and 36 h runs. The NCEP reanalysed fields show maximum values of \mathbf{J}_1 and \mathbf{J}_2 at 0000 UTC 11 November and this is the *sensitivity time* used for all the sensitivity results presented in this study. This time is used as the initialization time for the adjoint, and so the derived sensitivities are, in a strict sense, linked to the forecast for that time only. In practice, despite the fact that it is not guaranteed by the adjoint system, it is expected that a perturbation intended to increase \mathbf{J}_1 and \mathbf{J}_2 at the sensitivity time will intensify the whole cyclonic development.

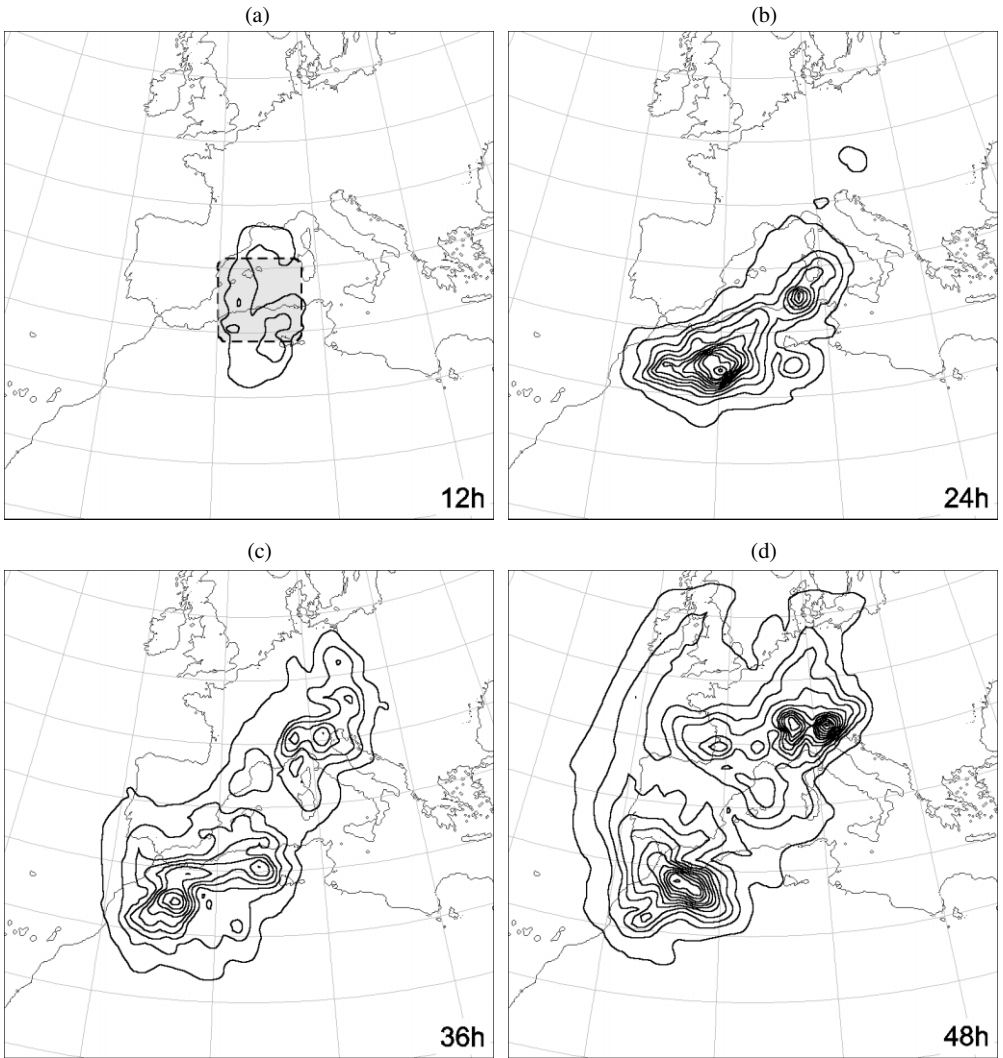


Figure 5. Vertical averages of the absolute values of the sensitivities to the response function \mathbf{J}_1 for all fields, for simulation runs of different durations ending at the sensitivity time (0000 UTC 11 November): (a) 12 h; (b) 24 h; (c) 36 h, and (d) 48 h. Units of the field are non-physical ($\text{s}^{-1}/[\text{model input}]$). Contour intervals are two units, with the lowest, outermost, contour being +2. In panel (a), the stippled square shows the location of the $600 \times 600 \text{ km}^2$ horizontal extent of \mathbf{J}_1 around the centre of the cyclone in the control simulation.

(a) Vorticity sensitivities (\mathbf{J}_1)

The adjoint model is run for the 12 h, 24 h, 36 h and 48 h time spans, using the vorticity response function (\mathbf{J}_1). The sensitivities to the initial conditions for each of these simulations are obtained. In order to summarize the three-dimensional sensitivity fields, a vertical average of the absolute values of the adjoint variables \hat{u} , \hat{v} , \hat{T} , \hat{p} and \hat{q} is shown in Fig. 5. While this field has no physical meaning in terms of sensitivity to specific perturbations, it provides a very good indication of the sensitivity distribution across the domain. As expected, the sensitivity field intensifies and spreads out with increasing simulation time. The 12 h field shows a relatively weak signal, highlighting

the surface cold front and vorticity maximum associated with the trough aloft, on the southern side of the cyclone over north Algeria (Fig. 5(a)). The sensitive areas for the 24 h simulation (Fig. 5(b)) correspond to the cold and warm surface fronts, enhanced over north Africa by the upper-level trough. For the 36 h run (Fig. 5(c)) the sensitivities spread northward dramatically, highlighting both the downstream side of the upper-level trough and the general area of cold advection ahead of the cold front across the Mediterranean basin and northern Spain (see Fig. 2(a,b)). Finally, the sensitivities for the 48 h simulation are related to the same features as the 36 h run, but reflect their temporal shift to the north-west (Fig. 5(d)). Therefore, the Moroccan and Algerian coast lands, together with south-western Europe, emerge as important sensitive areas for the intense cyclonic formation. It is noteworthy that no significant sensitivity is found over inland north Africa, the central Mediterranean or the Atlantic Ocean.

In order to assess the vertical distribution of the sensitivities and the relative impact of each of the prognostic variables, the results are partitioned by level and adjoint variable in Fig. 6. Note the difference in units of each of the curves. Whereas all refer to the same response function J_1 , each one indicates the expected change in the response function to perturbations of the corresponding field in the forward simulation. Comparing sensitivities shown by a forecast aspect to different fields, such as the wind components or the temperature, cannot be directly addressed using only the adjoint results. We need to define a unitary perturbation, in order to establish a relation between the fields. Once we define a perturbation, the sensitivities provide (in a linear sense) the effect of this perturbation on the response function. However, the relative importance of these individual effects on the response function, i.e. the question 'to which field is the response function most sensitive?', critically depends on the relative weight of each field in the definition of the unitary perturbation. A useful measure of the relative importance of the fields could be provided by the typical analysis error. This error, taken as a unitary perturbation, together with the indication of the effect of the perturbation on the response function as derived from the adjoint, would result in a meaningful comparison of the relative sensitivities shown by the response function to the various model input fields. Since the analysis error is an unknown quantity, however, a sensible practical estimation is used in this study. When comparing sensitivities to model input fields and when building perturbations (Eq. (1)), the same weight (s_i) will be given to 1 m s^{-1} , 1 K , 1 hPa and 1 g kg^{-1} and so a direct comparison among the curves in Fig. 6 is indicative.

A common feature among the simulations is the sensitivity shown to the temperature and specific humidity fields, which is 4–6 times greater than that obtained for the wind and pressure fields. This suggests that perturbations to the temperature and humidity fields over the areas where the main features of the event (low-level cold and warm fronts, upper-level trough and diabatic heating from condensation) evolve will have a larger impact on the response function than the other fields. This does not mean that the flow or pressure distributions are not important to this event, but recognizes the small importance of their precise representation on the initial fields with respect to the thermodynamic variables. Similar results, highlighting the importance of a correct representation of the low-level temperature field are described by Langland *et al.* (1995) in cyclogenesis and by Lewis *et al.* (2001) for the return flow over the Gulf of Mexico. For the 12 h simulation (Fig. 6(a)), the sensitivities are very weak and evenly distributed below $\sigma \approx 0.45$ ($\sim 500 \text{ hPa}$). However, the maximum sensitivities occur at low levels, indicating that the representation of the low-level frontal structures is relatively important for the 12 h run. The impact of perturbations in mid-levels becomes important for the longer runs and, despite the smaller relative response near the surface, low-level

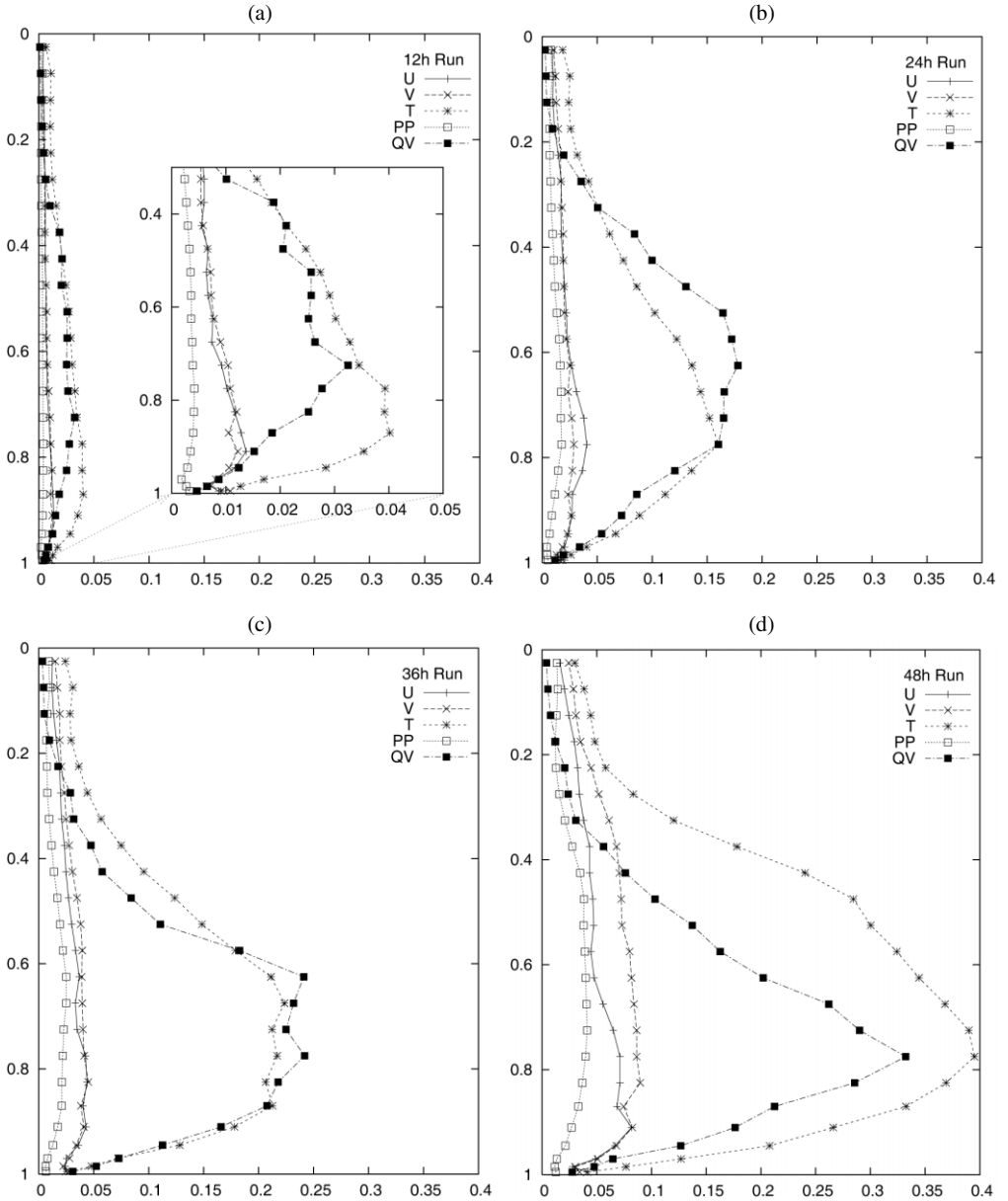


Figure 6. Vertical profiles of σ -average values of the sensitivities of the quantities u , v , T , p and q to the response function J_1 , for simulation runs of different durations ending at the sensitivity time (0000 UTC 11 November): (a) 12 h; (b) 24 h; (c) 36 h, and (d) 48 h. Units are $s^{-1}/(m s^{-1}) = m^{-1}$ for u and v , $s^{-1}K^{-1}$ for T , $s^{-1}/(hPa)$ for p and $s^{-1}/(g kg^{-1})$ for q . To better illustrate the variation of the various sensitivities with σ near the bottom left of panel (a), the inset shows sensitivities in the range up to 0.05 expanded fivefold.

($\sigma \sim 0.9\text{--}0.7$) features remain influential for all the simulation times. Although the sensitivities to q and T are likely to have large nonlinear components from the convective and microphysics processes, the linear results suggest that both these fields are important influences on the formation of the cyclone. On the other hand, it is noteworthy that while for the 12 h, 24 h and 36 h simulations the u and v components have similar relative impacts, for the longer 48 h run the v component has acquired a greater sensitivity (Fig. 6(d)). This is consistent with attributing a key role to the short upper-level trough and low-level northerly cold advection in the event (see Fig. 2(a,b)).

We now examine the spatial structure of the sensitivities to the two most representative fields, T and q , for the \mathbf{J}_1 response function. The sensitivity to T obtained for the 48 h run at $\sigma = 0.77$ (~ 800 hPa) shows that the main sensitivity areas are basically located south and south-east of the thermal trough, where maximum cold advection occurs (Fig. 7(a)). A perturbation built with this shape will produce an amplification of the already existing short thermal wave over southern Spain and a corresponding increase of cold advection through an intensification of the thermal gradient. As a consequence, baroclinic instability at low levels will be strengthened. On the other hand, the sensitivity obtained over southern France and the Alps highlights the effect on the cyclone's vorticity of the air which interacts with the cyclone as it later evolves northwards towards the western Mediterranean basin. Combined, the increase of the low-level cold advection and the modification of the shape and location of the upper cut-off low, act to intensify the upward motion and further intensify the low-level baroclinic development. The details of the T field along the leading edge of the trough are the features showing the maximum potential influence on \mathbf{J}_1 among the four time spans (Fig. 6(a)). Likewise, the role of q in the event also is highlighted, showing the largest values of \hat{q} at higher levels even for the 24 h run than seen from \hat{T} (Fig. 6(c)). The sensitivity to q at $\sigma = 0.625$ (~ 660 hPa) for the 24 h simulation again indicates that the sensitivity areas are mainly located along a region of large gradients of the field (Fig. 7(b)). Note that the adjoint results for north Africa indicate that a weakening of an already weak local gradient of q will favour a more intense cyclone development (i.e., increase of \mathbf{J}_1 24 h later). The physical interpretation of such a perturbation is not obvious, but is related to the mesoscale details of the sharp low-level q gradient associated with the cyclone, clearly identifiable during the next hours in the 24 h nonlinear simulation (not shown).

(b) Wind speed sensitivities (\mathbf{J}_2)

Results obtained when the adjoint model is initialized using $\nabla\mathbf{J}_2$ are similar and consistent with the fields shown in Figs. 5 and 6 for \mathbf{J}_1 though some important differences emerge. During the first 24 h, the \mathbf{J}_2 sensitivity regions are mostly located over the western Mediterranean Sea and stretch farther northward than the \mathbf{J}_1 sensitivity fields (Fig. 8). A notable difference between the \mathbf{J}_2 results and the \mathbf{J}_1 results is the inclusion of the northeastern side of the western Mediterranean in the \mathbf{J}_2 results, even for the short simulations. This may simply be because the response function is farther north, but it also reveals the effect of the important orographic ranges present along the northern boundary of the Mediterranean basin on the low-level flow (e.g., Buzzi and Tibaldi 1978; Bessemoulin *et al.* 1993). Again, \hat{T} and \hat{q} are the fields that the simulations consistently show have the largest sensitivities. For the sake of brevity, the average of \hat{T} and \hat{q} , and \hat{u} , \hat{v} and \hat{p} have been plotted for every time interval (Fig. 8(b)). The largest signals are found at mid-low levels, between $\sigma = 0.5$ and 0.9 . Unlike the \mathbf{J}_1 results, the longest run does not show the largest sensitivities. Instead, the 36 h simulation shows sensitivities 3 times larger than those from 48 h at mid-low levels. That is, a larger

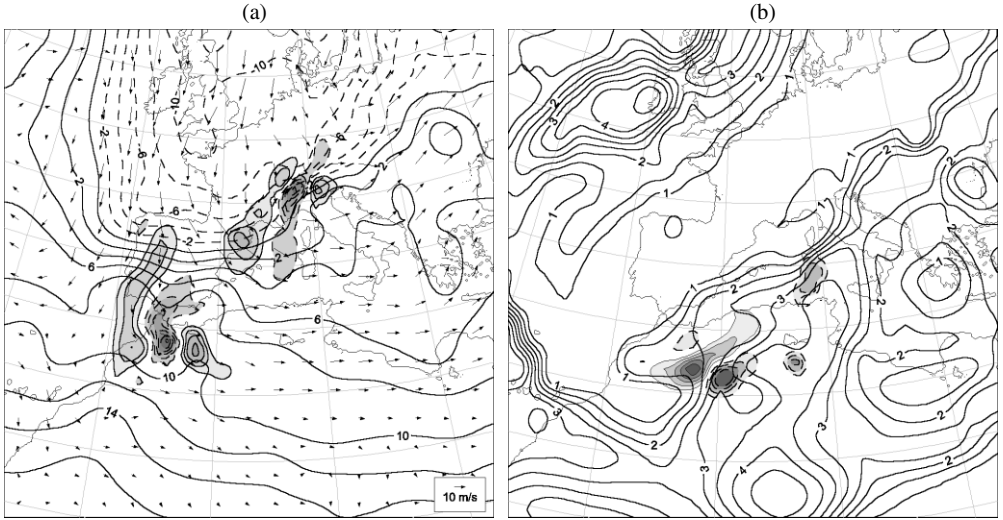


Figure 7. Sensitivity ($\nabla J_1 / t_0$) (stippled, with zero contour omitted and negative contours dashed) at σ levels and corresponding initial condition fields: (a) for 0000 UTC 9 November 2001 (ST - 48 h), \hat{T} ($s^{-1}K^{-1}$, contour interval $2 s^{-1}K^{-1}$) at $\sigma = 0.77$, and T (K, contour interval 2 K, negative contours dashed) and wind vector ($m s^{-1}$) at 800 hPa, and (b) for 0000 UTC 10 November 2001 (ST - 24 h), \hat{q} ($s^{-1}/(g kg^{-1})$, contour interval $0.5 s^{-1}/(g kg^{-1})$) at $\sigma = 0.625$ and q ($g kg^{-1}$, contour interval $0.5 g kg^{-1}$) at 650 hPa.

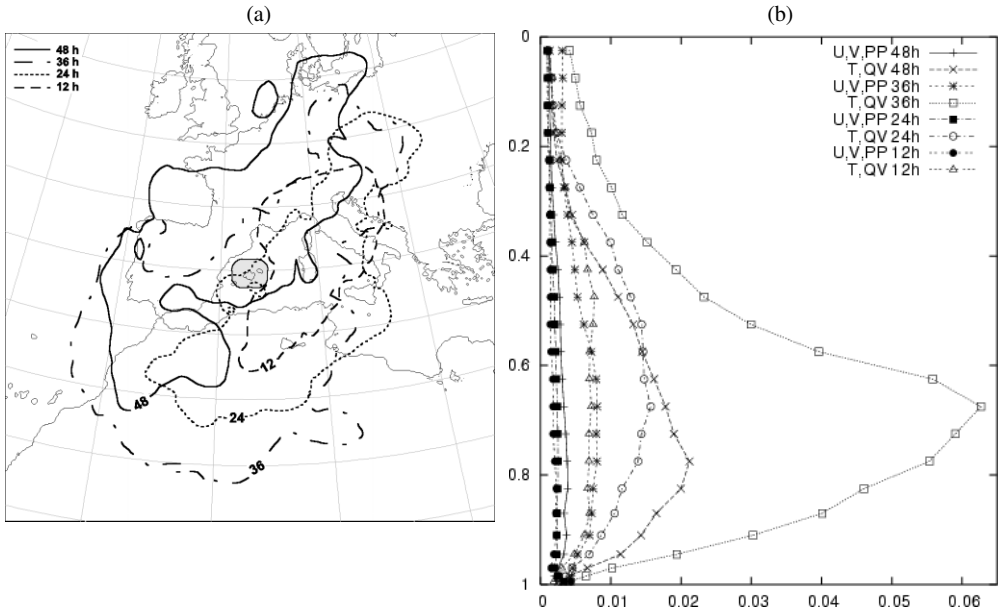


Figure 8. Sensitivities to response function J_2 : (a) contours of $([0.25 m s^{-1}]/[input fields])$ of the vertical average of all sensitivity fields for each of the 12 h, 24 h, 36 h and 48 h simulations (all ending at the sensitivity time (0000 UTC 11 November)) (the stippled area shows the extent of the area B used in defining J_2 (Eq. (3))), and (b) vertical profile of σ -average values of the sensitivities of the quantities u, v, T, p and q to the response function J_2 , for each of the simulations (units along the horizontal axis are non-physical ($s^{-1}/[input field]$)).

perturbation is required in the 48 h run than in the 36 h in order to obtain a similar response in the wind field over the Balearics. This is probably a reflection of the different trajectory followed by the 48 h run in comparison to the shorter runs. As seen in Fig. 4, the 48 h simulation does not capture the intense cyclone formation well, reducing the strength of the baroclinic zone and the intensity of the associated convection. Thus, the size of the perturbation needed to obtain a change in the winds around the Balearics must be much larger than in the cases where fast-growing modes are activated, such that the resulting sensitivity is weaker. In fact, a comparison between the 12 h forecast fields from the 48 h run and the initial conditions for the 36 h run shows differences of up to 3°C and 2 g kg^{-1} at 650 hPa in the location where the 36 h simulation shows large sensitivity.

(c) ADJ v. FWD perturbations

To analyse the actual effect of ADJ derived perturbations in the full nonlinear model, we perform experiments using perturbations built from the obtained sensitivities, using Eq. (1). Forecast fields are compared with the control runs to obtain the nonlinear forecast perturbations, which can be contrasted to the adjoint linear estimation (Zou *et al.* 1997; Langland *et al.* 1999a). We show three examples of perturbations derived from the vorticity response function (\mathbf{J}_1) to illustrate the general response of the nonlinear model with respect to the linear estimation (Fig. 9). Since the moist physics was shown to decrease the linear model's accuracy with the TGL–FWD correlation method presented in section 4, a first experiment perturbing the q field of the 24 h run is designed. In this experiment $s_q = 1\text{ g kg}^{-1}$ and $s_i = 0$ otherwise in Eq. (1), with $\alpha = 1$. This perturbation, as derived from the sensitivity fields, is expected to intensify the cyclonic development and is located in the mid-levels over a region of large gradient of q over north Africa (Fig. 7(b)). The nonlinear perturbed simulation shows a decrease in the surface pressure of 3 hPa over the Balearic Islands, which helps to extend the cyclone westward instead of deepening its central pressure (which only decreased by 1 hPa). The wind field at low levels changes according to the modified cyclone shape, enlarging and shifting the low-level jet to the north-west, north of the Balearic Islands. In addition, \mathbf{J}_1 increases from a value of 7.94 s^{-1} in the control run to 8.62 s^{-1} in the perturbed run. Results from the opposite forecast perturbation (i.e., $\alpha = -1$), show similar opposite perturbations, indicating the skill of the adjoint model in determining not only the sensitivity areas of the cyclone, but also the sign of the perturbation in the forecast field. These simulations, in which only the q field is perturbed, confirm the important sensitivity of the cyclone simulation to the moist processes, relativising the uncertainties associated with the moist processes in the linear models inferred in section 4.

On the other hand, the temperature field is highlighted as the field showing the largest sensitivity in the simulations. The large sensitivities seen in the 36 h linear model results (Fig. 8(b)) motivate the detailed analysis of the actual response of the nonlinear model to the derived perturbation of the temperature field. Here, $s_T = 1\text{ K}$ and $s_i = 0$ otherwise, with $\alpha = 1$. This perturbation mainly affects the low-to-mid levels and is located along the south and south-east edges of the cold trough, similar to the structure shown in Fig. 7(a), but 12 hours later. Again, the perturbed simulation produces a deeper cyclone that is shifted to the west, and a consequent shift to the north-west of the low-level jet (Fig. 9(b)). Results from $\alpha = -1$ also show an opposite direction in the forecast perturbations. Although the response obtained was of the correct sign and in the correct location, the amplitude of the nonlinear perturbation is weaker than that expected from the relatively large sensitivity predicted by the adjoint. An important feature of this perturbed simulation is that the modification of the thermal front intensifies and moves

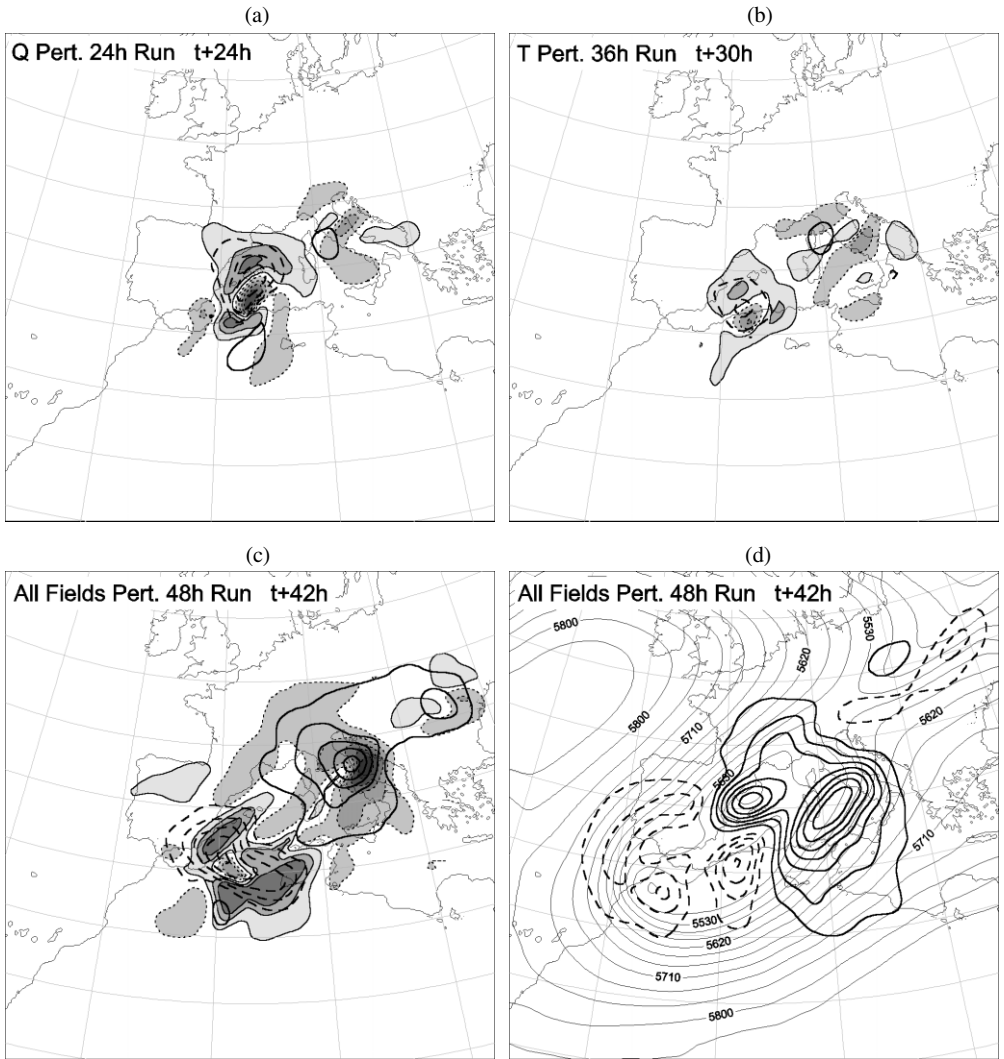


Figure 9. Nonlinear forecast perturbations (perturbed minus control) from J_1 sensitivities, built putting $\alpha = 1$ in Eq. (1) (dashed contours show negative values and zero contours are omitted): (a) sea-level pressure (hPa, unstippled, contour interval 1 hPa) and wind speed (m s^{-1} , stippled, contour interval 2 m s^{-1}) at 850 hPa 0000 UTC 11 November 2001 for perturbations built with $s_q = 1 \text{ g kg}^{-1}$ and other $s_i = 0$; (b) sea-level pressure (hPa, unstippled, contour interval 1 hPa) and wind speed (m s^{-1} , stippled, contour interval 2 m s^{-1}) at 850 hPa 1800 UTC 10 November 2001 for perturbations built with $s_T = 1 \text{ K}$ and other $s_i = 0$; (c) sea-level pressure (hPa, unstippled, contour interval 1 hPa) and wind speed (m s^{-1} , stippled, contour interval 2 m s^{-1}) at 850 hPa 1800 UTC 10 November 2001 for perturbations built with all $s_i = 1$ (in their respective units), and (d) geopotential height of the 500 hPa surface (m, thin lines, contour interval 30 m) of the 48 h control run, valid 1800 UTC 10 November, and nonlinear perturbations (m, thick lines, contour interval 5 m).

the upper-level cut-off low to the south-west for $\alpha = 1$ and weakens and shifts it to the north-east for $\alpha = -1$. In addition, a faster evolution of the upper-level trough and its associated effect at low levels is observed in the perturbed simulation. As a consequence, the maximum change in wind speed over the Balearic Islands is not observed at the sensitivity time (+36 h, 0000 UTC 11 November) but earlier, at about +30 h (1800 UTC 10 November, Fig. 9(b)), when the perturbed system crosses the region. Here, although the cyclogenesis has been intensified, nonlinear effects lead to a shift of the cyclone in

space and time, so that the nonlinear model forecast does not reproduce the expected perturbation at the sensitivity time over the targeted region. Such behaviour introduces challenges to the quantitative testing of the adjoint results in terms of the nonlinear response function (Lewis *et al.* 2001). For example, the perturbations introduced to a simulation at upper levels, intended to deepen the surface cyclone, probably enhance the upper-level trough vorticity and temperature advection, not only producing a deeper surface cyclone, but also a faster moving system, and so eventually moving the system under study out of the target region (i.e., moving the cyclone out of regions A and B for \mathbf{J}_1 and \mathbf{J}_2).

Finally, the response of the inaccurate 48 h run to the perturbations is analysed. In this experiment, $\alpha = 1$ and s_i are all set to their corresponding unitary values, so that u , v , T , p and q fields are perturbed. Much as in the previous experiment, the perturbed run produces a faster evolution of the surface systems, and the maximum changes seen over the area of interest are obtained earlier in the run. A notable deepening of 5 hPa is obtained to the south-west of the western Mediterranean (Fig. 9(c)) and an increase in the low-level wind speeds of 6 m s^{-1} over the area is seen. These differences are attributed to a change in the upper-level trough, which has shifted the dynamic forcing from the north-eastern to the south-western side of the basin (Fig. 9(d)). In fact, the effect of the applied perturbation on the trough is to intensify the generation of the two isolated centres already identified in Fig. 2(c). These centres are diagnosed as important structures in the evolution of the cyclone by Arreola *et al.* (2003), and that they are missed in the 48 h unperturbed run may explain the inaccurate reproduction of the cyclonic development in this simulation. A comparison of the Petterssen (1956) frontogenetic parameter at low levels over north Africa during the latter hours of simulation shows areas with an increase of $8 \times 10^{-9} \text{ }^\circ\text{C s}^{-1}\text{m}^{-1}$ in the perturbed simulation (not shown), confirming the strengthening of the baroclinic instability and suggesting its relation with the details of the upper-level trough evolution.

Therefore, case by case analysis of the perturbed runs reveals the helpful guidance of the adjoint results and provides several reasons, such as spatial and temporal shift of targeted structures, that may explain some of the degradation detected in the results of the objective validation presented in section 4.

6. CONCLUSIONS

The analysis of the sensitivities shown by the numerical forecast of an intense Mediterranean cyclone is presented. The typical path followed by this type of Mediterranean cyclone crosses areas with few observations, such as the Mediterranean Sea, the north African region and the Atlantic Ocean.

The adjoint of the tangent linear version of the MM5 is used to determine the areas of sensitivity. A first exploratory analysis of the accuracy of the linear model in reproducing the evolution of the perturbations in the nonlinear model is made using the tangent linear model. Correlations between tangent linear and nonlinear forecasts reveal that, for the simulation of this intense cyclone, the linear model reproduces with acceptable accuracy the evolution of perturbations with amplitudes of the typical analysis error. However, moist physics introduces nonlinearities through decision points in the model trajectory which are difficult to anticipate using the tangent model. The convective scheme is shown to produce unexpected, yet relatively important, structural instabilities in the tangent linear model (detected at the very small perturbation sizes), and diabatic heating from simple stratiform condensation is also shown to hamper the linear model accuracy. Once the application range for the linear results is analysed,

sensitivity fields for four time spans, 12 h, 24 h, 36 h and 48 h, are computed. Two response functions are used to characterize the cyclone's intensity in the sensitivity analysis: vorticity around the cyclone centre at low levels, and wind speed at the surface over the Balearic Islands. These functions focus upon both a general dynamic aspect and a more particular mesoscale feature that are directly related to the reported damage in the region. Sensitive areas for the shorter 12 h and 24 h simulations are mainly located over north Africa and the Mediterranean Sea, showing large sensitivity in the lower to middle tropospheric levels. For the longer, 36 h and 48 h simulations, the sensitivities extend toward western Europe, with signals also over the Alpine region, where a sensitivity to the short-wave features at middle levels is highlighted. Despite an increase in the response at mid-to-upper levels as integration time increases, the low levels (about 800 hPa) have the largest sensitivities for all four time spans. Results show that the largest sensitivities occur for the temperature and specific-humidity fields, especially in association with subsynoptic-scale features along the cold front associated with the trough at mid-to-low levels and over a tight gradient of specific humidity moving over north Africa during the simulations.

A direct method is used to evaluate the effect of the adjoint derived sensitivities in the nonlinear model. Control runs are perturbed using the information from the adjoint and then the nonlinear forecast perturbations are analysed. Perturbation sizes are chosen according to the validation conclusions, and the results show that all perturbations produce the estimated response in the forecast, although the forecast perturbations are sometimes weaker or shifted in space and time. These perturbed simulations confirm the sensitivity shown by the nonlinear simulations to the precise shape of the mid-to-upper level trough, the generation of the baroclinic zone, and the details of a large specific-humidity gradient region at mid-to-low levels over north Africa. These runs also illustrate the ability of the adjoint not only to detect the areas of important sensitivity but also to provide valuable guidance in building perturbations intended to modify the forecast in a certain direction, i.e. to intensify or attenuate the cyclonic development.

From an operational perspective, the improvement in the originally poor 48 h forecast is particularly remarkable. Whereas the 48 h control run does not accurately reproduce the shape and intensity of the cyclone, a perturbation built following the adjoint guidelines modifies the original initial conditions in such a way that the upper-level trough, important in the event, is more accurately represented and a better prediction of the cyclone's surface parameters is obtained.

Therefore, in addition to indicating the areas and levels where a better description of the atmospheric variables would efficiently improve the numerical simulation of this type of event, this study points out the possible use of the adjoint-derived sensitivities in building convenient realistic initial condition perturbations for applications such as ensemble forecasting.

ACKNOWLEDGEMENTS

This work was performed while the first author held a National Research Council Research Associateship Award at the NOAA/National Severe Storms Laboratory. This research was mainly developed in the framework of the WMO-WWRP 'Mediterranean Experiment MEDEX' and MEDEXIB (REN2000-03482, Spain) projects. Computer support provided by NCAR/Scientific Computer Division (which is sponsored by the National Science Foundation) for model data preprocessing is also acknowledged. The authors especially acknowledge Dr R. H. Langland, J. Lewis, K. Raeder, Dr A. Buzzi and the two anonymous reviewers for their helpful comments which have helped to improve this text substantially.

REFERENCES

- Alpert, P., Krichak, S. O., Krishnamurti, T. N., Stein, U. and Tsidulko, M. 1996 The relative roles of lateral boundaries, initial conditions, and topography in mesoscale simulations of lee cyclogenesis. *J. Appl. Meteorol.*, **35**, 1091–1099
- Arreola, J., Homar, V., Romero, R., Ramis, C. and Alonso, S. 2003 ‘Multiscale numerical study of the 10–12 November 2001 strong cyclogenesis event in the Western Mediterranean’ in *Plinius Conference on Mediterranean Storms IV*, p. Sec. 1 num 30, European Geophysical Society
- Benjamin, S. G. 1983 ‘Some effects of heating and topography on the regional severe storm environment’. Ph.D. thesis, The Pennsylvania State University. Available from University Microfil, 300 N. Zeeb Rd., P.O. Box 1346, Ann Arbor, MI 46801-1346, USA
- Bessemoulin, P., Bougeault, P., Genovés, A., Jansà, A. and Puech, D. 1993 Mountain pressure drag during PYREX. *Beitr. Phys. Atmos.*, **66**, 305–325
- Buzzi, A. and Tibaldi, S. 1978 Cyclogenesis in the lee of the Alps: A case study. *Q. J. R. Meteorol. Soc.*, **104**, 271–287
- Dudhia, J. 1989 Numerical study of convection observed during the winter monsoon experiment using a mesoscale two-dimensional model. *J. Atmos. Sci.*, **46**, 3077–3107
- Dudhia, J., Gill, D., Guo, Y.-R., Manning, K., Bourgeois, A. and Wang, W. 2002 ‘PSU/NCAR Mesoscale Modeling System: Tutorial Class notes and User’s Guide: MM5 Modeling System Version 3’. Available from NCAR, Boulder, USA
- Errico, R. M. 1997 What is an adjoint model? *Bull. Am. Meteorol. Soc.*, **78**, 2577–2591
- Errico, R. M. and Raeder, K. D. 1999 An examination of the accuracy of the linearization of a mesoscale model with moist physics. *Q. J. R. Meteorol. Soc.*, **125**, 169–195
- Errico, R. M. and Vukićević, T. 1992 Sensitivity analysis using an adjoint of the PSU-NCAR mesoscale model. *Mon. Weather Rev.*, **120**, 1644–1660
- Errico, R. M., Vukićević, T. and Raeder, K. 1993 Examination of the accuracy of a tangent linear model. *Tellus*, **45A**, 462–477
- Grell, G. A., Dudhia, J. and Stauffer, D. R. 1995 ‘A description of the fifth-generation Penn State/NCAR mesoscale model (MM5)’. NCAR Tech. Note NCAR/TN-398+STR, Boulder, USA
- Homar, V., Ramis, C. and Alonso, S. 2002 A deep cyclone of African origin over the western Mediterranean: Diagnosis and numerical simulation. *Ann. Geophys.*, **20**, 93–106
- Jansà, A., Genovés, A., Picornell, M. A., Campins, J., Riosalido, R. and Carretero, O. 2001 Western Mediterranean cyclones and heavy rain. *Meteorol. Appl.*, **8**, 43–56
- Kato, T. 1980 *Perturbation Theory for Linear Operators. 2nd Edition*. Springer-Verlag, Berlin, Germany
- Kuo, H. 1974 Further studies of the parameterization of the influence of cumulus convection on large-scale flow. *J. Atmos. Sci.*, **31**, 1232–1240
- Langland, R. 1999 Summary of an informal workshop on targeted observations for extratropical and tropical forecasting. *Bull. Am. Meteorol. Soc.*, **80**, 2331–2338
- Langland, R. H., Elsberry, R. and Errico, R. M. 1995 Evaluation of physical processes in an idealized extratropical cyclone using adjoint sensitivity. *Q. J. R. Meteorol. Soc.*, **121**, 1349–1386
- Langland, R. H., Gelaro, R., Rohaly, G. D. and Shapiro, M. A. 1999a Targeted observations in FASTEX: Adjoint-based targeting procedures and data impact experiments in IOP17 and IOP18. *Q. J. R. Meteorol. Soc.*, **125**, 3241–3270
- Langland, R. H., Toth, Z., Gelaro, R., Szunyogh, I., Shapiro, M., Majumdar, S. J., Morss, R. E., Rohaly, G. D., Velden, C., Bond, N. and Bishop, C. H. 1999b The North Pacific Experiment (NORPEX-98): Targeted observations for improved North American weather forecasts. *Bull. Am. Meteorol. Soc.*, **80**, 1363–1384
- Langland, R., Shapiro, M. A. and Gelaro, R. 2002 Initial condition sensitivity and error growth in forecasts of the 25 January 2000 east coast snowstorm. *Mon. Weather Rev.*, **130**, 957–974
- Lewis, J. M., Raeder, K. D. and Errico, R. M. 2001 Vapor flux associated with return flow over the Gulf of Mexico: a sensitivity study using adjoint modeling. *Tellus*, **53A**, 74–93

- Molteni, F., Buizza, R., Palmer, T. N. and Petroliagis, T. 1996 The ECMWF Ensemble Prediction System: Methodology and validation. *Q. J. R. Meteorol. Soc.*, **122**, 73–119
- Park, S. K. and Droegemeier, K. K. 1997 Validity of the tangent linear approximation in a moist convective cloud model. *Mon. Weather Rev.*, **125**, 3320–3340
- Petterssen, S. 1956 *Weather analysis and forecasting (vol I)*. McGraw-Hill Company, New York, USA
- Shay-El, Y. and Alpert, P. 1991 A diagnostic study of winter diabatic heating in the Mediterranean in relation to cyclones. *Q. J. R. Meteorol. Soc.*, **117**, 715–747
- Snyder, C. 1996 Summary of an informal workshop on adaptive observations and FASTEX. *Bull. Am. Meteorol. Soc.*, **77**, 953–961
- Toth, Z. and Kalnay, E. 1993 Ensemble forecasting at NMC: The generation of perturbations. *Bull. Am. Meteorol. Soc.*, **74**, 2317–2330
- Vukićević, T. and Errico, R. M. 1993 Linearization and adjoint of parameterized moist diabatic processes. *Tellus*, **45A**, 493–510
- Xu, M., Stensrud, D. J., Bao, J.-W. and Warner, T. T. 2001 Applications of the adjoint technique to short-range ensemble forecasting of mesoscale convective systems. *Mon. Weather Rev.*, **129**, 1395–1418
- Zhang, D. L. and Anthes, R. A. 1982 A high-resolution model of the planetary boundary layer-sensitivity tests and comparisons with sesame-79 data. *J. Appl. Meteorol.*, **21**, 1594–1609
- Zou, X., Vandenbergh, F., Pondeca, M. and Kuo, Y.-H. 1997 'Introduction to adjoint techniques and the MM5 adjoint modeling system'. NCAR Tech. Note NCAR/TN-435+IA, Boulder, USA
- Zou, X., Huang, W. and Xiao, Q. 1998 'A User's Guide to the MM5 Adjoint Modeling System'. NCAR Tech. Note NCAR/TN-437+IA, Boulder, USA